Distribution Agreement

In presenting this thesis or dissertation as a partial fulfillment of the requirements for an advanced degree from Emory University, I hereby grant to Emory University and its agents the non-exclusive license to archive, make accessible, and display my thesis or dissertation in whole or in part in all forms of media, now or hereafter known, including display on the world wide web. I understand that I may select some access restrictions as part of the online submission of this thesis or dissertation. I retain all ownership rights to the copyright of the thesis or dissertation. I also retain the right to use in future works (such as articles or books) all or part of this thesis or dissertation.

Signature:

_____ _____

Xucheng (Fred) Huang Date

Analysis of Simultaneous Eye-tracking and fMRI Data Collected in Children with ASD

By

Xucheng (Fred) Huang
Master of Public Health

Department of Biostatistics & Bioinformatics

Benjamin Risk, Ph.D.
Committee Chair

Tianwen Ma, Ph.D.
Committee Member

Analysis of Simultaneous Eye-tracking and fMRI Data Collected in Children with ASD

By

Xucheng (Fred) Huang
B.E., Northwest A&F University (NWAFU), China, 2017

Thesis Committee Chair: Benjamin Risk, Ph.D.

An abstract of
A thesis submitted to the Faculty of the
Rollins School of Public Health of Emory University Emory University
in partial fulfillment of the requirements for the degree of
Master of Public Health
in Department of Biostatistics & Bioinformatics
2024

Abstract

Analysis of Simultaneous Eye-tracking and fMRI Data Collected in Children with ASD
By Xucheng (Fred) Huang

Functional magnetic resonance imaging (fMRI) is a useful tool for understanding the complexities of brain activity, particularly in children with autism spectrum disorder (ASD). While recent studies have examined dynamic connectivity in ASD using resting-state fMRI, analyzing dynamic connectivity of task-based fMRI may offer novel insights. To enhance our understanding of brain connectivity in ASD, this thesis has two aims: 1) analyze the relationship between eye-tracking data and movie-watching tasks in children with and without ASD using the general linear model; 2) develop a novel model for analyzing dynamic connectivity during a task. For aim 1, we develop an analytic pipeline for convolving eye-blink and eye-fixation events with the Hemodynamic Response Function (HRF), which is then analyzed using conventional task-based modeling approach. For aim 2, we propose a novel covariance regression in which we estimate the association between time-varying correlations between brain regions and the eye-tracking data. We analyzed 12 ASD children and 22 non-ASD children collected in the Brain Connectivity Study at Emory University. Brain activation was significantly lower in ASD during eye-fixation events in regions associated with sensory processing, attention networks, auditory processing, executive functions, and language processing. The covariance regression analysis further identified large individual variability in functional connectivity among the ASD group. Our two-stage modeling approach extends beyond studies of ASD, providing an analytical framework to complement traditional task-based fMRI analyses with dynamic connectivity modeling.

Keywords: covariance regression, dynamic connectivity, functional connectivity analysis, naturalistic movie watching

Analysis of Simultaneous Eye-tracking and fMRI Data Collected in Children with ASD

By

Xucheng (Fred) Huang
B.E., Northwest A&F University (NWAFU), China, 2017

Thesis Committee Chair: Benjamin Risk, Ph.D.

A thesis submitted to the Faculty of the
Rollins School of Public Health of Emory University
in partial fulfillment of the requirements for the degree of
Master of Public Health
in Department of Biostatistics & Bioinformatics
2024

Acknowledgments

This research was supported in part by the National Institute of Mental Health of the National Institutes of Health under award number R01 MH129855. The content is solely the responsibility of the authors and does not necessarily represent the official views of the National Institutes of Health.

1 Introduction

Autism spectrum disorder (ASD) is a neurodevelopmental condition characterized by social and communication deficits and repetitive behaviors, which affects approximately one in 36 children in the United States (Maenner, 2023). Functional MRI (fMRI) has been a traditional tool in ASD research. It measures the blood-oxygen-level-dependent (BOLD) signal over time, which is an indirect indicator of neural activity. This technique enables researchers to study brain functional connectivity (Friston et al., 1993), or the correlations in BOLD signals between different brain regions (Biswal et al., 2010), offering insights into how different areas of the brain interact during various tasks or at resting state. Studies using resting-state fMRI (rs-fMRI), where participants are instructed to lie motionless and focus on a crosshair, have identified differences in functional connectivity between ASD and non-ASD participants (Hull et al., 2017). However, task-based fMRI studies are considered by some investigators to be more relevant for understanding the neural mechanisms in patient populations (Huijbers et al., 2017; Greene et al., 2018; Elliott et al., 2019; Zhao et al., 2023). Previous task-based fMRI studies of ASD suggest that individuals with ASD show atypical activation in language and working memory networks, including stronger activation in Broca's area, altered deactivation in the cerebellum and temporal areas, alongside evidence of compensatory mechanisms for maintaining performance, visual processing, auditory processing, language processing, executive function, and working memory. (Knaus et al., 2008; Braden et al., 2017; Eack et al., 2017; Rahko et al., 2016). Event-based task fMRI experiments reveal distinct brain activation related to object inspection and task context in ASD (Marsman et al., 2012).

Although these previous results are promising, there are limitations in the current methodologies, especially concerning functional connectivity analysis in fMRI studies. First, the analysis of dynamic connectivity in task fMRI has received little attention. Current task-based fMRI studies tend to overlook the investigation of dynamic interactions between brain regions. Such interactions are essential for a comprehensive understanding of ASD. Although some traditional approaches such as psychophysiological interaction (PPI) models (McLaren et al., 2012) and dynamic causal modeling (DCM) can be employed to examine task functional connectivity, they have challenges in either providing imprecise estimates (Di and Biswal, 2017) or are too complex for brain-wide studies (Friston et al., 2003). Second, participant motion is a significant issue in functional connectivity studies using resting-state fMRI, which has been shown to introduce bias (Satterthwaite et al., 2013). Additionally, current task activation studies primarily centers on static' tasks, like text reading and object recognitionmost (Park et al., 2020; Marsman et al., 2012), and they do not incorporate crucial task-related covariates in their models. Therefore, new approaches are needed for task-based fMRI studies.

To address experimental design limitations, this fMRI study employed movie-watching tasks with simultaneous eye-tracking. Children tend to move less when engaged in such tasks (Vanderwal et al., 2019; Rajagopal et al., 2014), reducing motion-related biases. Consequently, movie-watching tasks may be a more reliable alternative to traditional rs-fMRI studies (Huijbers et al., 2017; Meissner et al., 2020). The integration of brain activation and functional connectivity analyses during movie-watching tasks may provide insights into the

neural mechanisms underlying ASD.

Eye-tracking during a movie-watching task may provide insight into the brain regions that interact during engagement. Notably, previous studies outside the scanner have indicated that eye-blink rate patterns provide a reliable measure of individual engagement (Ranti et al., 2020), and eye-fixation events are closely linked to brain language processing areas and frontal control regions (Henderson et al., 2015). Eye-blinking has been used to define ASD subtypes prior to collecting rs-fMRI data, and these subtypes differed in their functional connectivity patterns (Lombardo et al., 2019). By incorporating eye-tracking information during the fMRI scan, we aim to gain insight into how engagement during movie watching is associated with brain activity and connectivity.

We propose a two-step approach to gain insight into the association between engagement during movie watching and brain activity. In aim 1, we model brain activation using the traditional general linear model (Friston et al., 1994). In our application, we construct our task covariates from eye-blink and eye-fixation events collected during the movie-watching tasks. In aim 2, we complement the brain activation study with a novel approach to covariance regression. This method facilitates the examination of dynamic functional connectivity through the residuals of task activation, modeling the residual covariance matrix time series as a linear function of both task-specific covariates and nuisance variables. Similar to covariance regression (Hoff and Niu, 2012), our outcome in this second aim is the conditional covariance matrix given covariates. However, the covariance model in Hoff and Niu (2012) is hard to interpret and possibly biologically implausible. It involves a quadratic form where negative and positive values of a covariate modify the covariance in the same way, rather than a simpler approach where covariances can increase with an increase in the covariate. Predicting covariance matrices is a goal in multivarate generalized autoregressive conditional heteroskedasticity models (MGARCH) (Lindquist et al., 2014; Engle, 2002), but these time-series models don't incorporate the effect of covariates.

We conducted an analysis of thirty-two participants (12 ASD) collected as part of the Brain Connectivity Study at Emory University, after removing those with low-quality eye-tracking data. Our approach involved convolving eye-blink and eye-fixation events with the hemodynamic response function (HRF) and analyzing them with an autoregressive model. This model helped us understand how individual brain regions respond to these eye movements. Then, we applied a novel covariance regression to further model the residuals left over from the first level autoregresive model. We employed log-Euclidean transformation on residual convariance matrices and fitting ordinary least squares (OLS) models for each brain connection edge. We utlized brain maps to visually present our findings. Finally, we discussed the results and limitations of our study in the concluding sections.

2 Dataset

2.1 MRI data and movie-watching task

This study was approved by Emory IRB 00003827. Participants were recruited from the Atlanta metropolitan area, including patients from the Marcus Autism Center. All participants received training in a mock MRI scanner using MoTrak software (Psychology

Software Tools, Pittsburgh, USA). The goal of the training session is to move < 3 mm in 6 minutes. Children completed up to five mock scan training sessions. Children were scanned when the team determined they were 1) able to tolerate being in the scanner for 35 minutes; 2) no safety concerns for participants, staff members, or equipment (e.g., elope risk, self-injurious behaviors, aggression, disruptive behavior). Movie-watching task fMRI was collected as part of a larger study including resting-state fMRI. Scan sessions included a T1 MPRAGE (1x1x1 mm^3 resolution, with TR/TE=2300/2.96 ms, and IPA (GRAPPA) factor of 2 with acquisition time 5:11 minutes), an AP and PA spin echo sequence, followed by rs-fMRI (3:36), a movie watching task (5:45), rs-fMRI (3:36), an optional break, repeated AP and PA spin echoes, rs-fMRI (3:36), movie watching task 2 (6:42), and rs-fMRI (3:36). All fMRI sequences were conducted using T2*-weighted runs with TR=1127 ms, 2.5 mm isotropic voxels, 60 slices, TE=32.2 ms, FA=51°, multiband factor=4, which a previous study found to be optimal for brain-wide functional connectivity (Risk et al., 2021). In some cases, children requested additional breaks, and additional AP and PA spin echoes were collected. Data were processed using fMRIPrep 21.0.2 with the cifti option for cortical surface representation of fMRI signals (Esteban et al., 2019). A "session" was defined by whether the participant left the scanner, with data organized in BIDS format such that the spin echoes from a session were used in the fMRIPrep distortion correction of fMRI data.

The movie-watching tasks were split into three segments for Task 1 and two for Task 2. The movie segments included excerpts from "The Sandlot" and "Welcome to the Dollhouse." For Task 1, the *0021 SAND* clip lasts 127 seconds, the *0023 DOLL* clip lasts 107 seconds, and the *0024 DOLL* clip lasts 66 seconds. Task 2 includes the *0022 SAND* clip, which lasts 238 seconds, and the *0025 DOLL* clip, lasting 134 seconds. Specifically, the *0021 SAND* and *0022 SAND* clips are sequential scenes showing children playing baseball from the film "The Sandlot." *0023 DOLL* is about a girl who is alone trying to find a seat in the cafeteria, *0024 DOLL* shows the same girl standing up to a boy cheating during an in-class exam, and *0025 DOLL* depicts the boy's reaction after being reported for attempting to cheat post-exam. Each watching task is preceded by a crosshair displayed for 3 seconds at the center of the screen, followed by a 15 seconds crosshair displayed between video clips, and ended with 12 seconds of the crosshair.

2.2 Eye-tracking data

We used EyeLink 1000 Plus (Version 5.03, SR Research Lnon-ASD. Ottawa, Ontario, Canada) as an eye-tracking tool, specifically designed without ferromagnetic materials, to record ocular movements with a high temporal resolution of 500 Hz. This equipment is fully compatible with fMRI technology. The EyeLink 1000 Plus software calculates the onsets and durations of eyeblinks, fixations, and saccades. Participants watched a total of five videos across two task sessions (Section 2.1) inside the scanner, which were delivered through professional edition of E-Prime software (E-Studio Version 2.0.10.252 for experiment design and Runtime Version 2.0.10.356 for execution).

Throughout the eye-tracking process, we recorded the task-specific quality of the data for each individual, based on the eye-tracking details such as calibration accuracy, validation results, and whether the participant's movement caused the head coil to cover the eyes. Based on these criteria, we categorized the eye-tracking data into three quality tiers: low, medium,

and high. Participants with low-quality eye-tracking data were excluded from our study. If an individual's eye-tracking data was of low quality during one of the movie-watching tasks, we only removed the data from that specific task session, while retaining and analyzing data from the other task session.

After completing the eye-tracking quality control procedures, our analysis encompassed data from 34 participants. Within this cohort, we had 12 children diagnosed with ASD and 22 non-ASD individuals. In the ASD group, 4 out of 12 participants are female, whereas the non-ASD group has 12 females out of 22 participants. For each participant, we computed the percentage duration of eye-blink and eye-fixation events across five video clips within two movie-watching tasks. Table 1 presents a detailed breakdown of these eye-tracking metrics for 34 participants, categorized by ASD group and gender.

	Movie 1			Movie 2	
	0021 SAND	**0023 DOLL**	**0024 DOLL**	**0022 SAND**	**0025 DOLL**
Eye-blink (Medain Percentage, Q1, Q3)					
ASD – Female (n = 4)	2.81 (2.59, 3.03) [n = 2]	6.22 (5.80, 6.64) [n = 2]	10.67 (10.05, 11.28) [n = 2]	17.95 (10.51, 23.49) [n = 3]	19.91 (10.98, 30.47) [n = 3]
ASD – Male (n = 8)	1.17 (0.79, 3.37) [n = 7]	3.86 (2.70, 4.63) [n = 7]	3.52 (2.96, 5.09) [n = 7]	1.29 (0.93, 1.54) [n = 4]	1.52 (1.39, 1.70) [n = 4]
TD – Female (n = 12)	2.13 (0.62, 3.34) [n = 11]	2.97 (0.94, 5.33) [n = 11]	2.68 (1.02, 4.80) [n = 11]	2.39 (1.23, 4.44) [n = 11]	2.33 (1.52, 4.17) [n = 11]
TD – Male (n = 10)	2.43 (0.93, 4.55) [n = 10]	5.33 (2.72, 8.18) [n = 10]	3.48 (2.31, 5.33) [n = 10]	2.25 (1.57, 6.04) [n = 10]	3.77 (2.38, 6.72) [n = 10]
Eye-fixation (Median Percentage, Q1, Q3)					
ASD – Female (n = 4)	85.56 (83.98, 87.13) [n = 2]	80.60 (79.92, 81.28) [n = 2]	73.55 (71.74, 75.35) [n = 2]	67.79 (66.97, 77.94) [n = 3]	64.58 (59.12, 77.46) [n = 3]
ASD – Male (n = 8)	92.04 (78.43, 92.83) [n = 7]	89.43 (76.78, 89.90) [n = 7]	89.43 (76.78, 89.90) [n = 7]	85.43 (75.98, 89.79) [n = 4]	82.74 (73.27, 86.96) [n = 4]
TD – Female (n = 12)	90.43 (88.41, 93.75) [n = 11]	87.73 (85.81, 90.08) [n = 11]	90.86 (85.44, 92.41) [n = 11]	90.71 (84.85, 92.90) [n = 11]	90.15 (83.31, 91.50) [n = 11]
TD – Male (n = 10)	89.46 (87.38, 92.35) [n = 10]	82.97 (79.10, 88.66) [n = 10]	86.89 (84.50, 89.64) [n = 10]	89.85 (85.14, 91.58) [n = 10]	88.45 (86.06, 89.79) [n = 10]

Table 1: Demographic table and summary of Eye-Blink and Eye-Fixation Measurements: the median percentages for the duration of eye-blink and eye-fixation, along with the first and third quartile ranges, for each video clip across different sexes and ASD and non-ASD groups.

3 Methods

3.1 Notation

Let $i \in \{1, \ldots, N\}$ represent the subject, $v \in \{1, \ldots, V\}$ denote the brain region, and $t \in \{1, \ldots, T\}$ index time within the fMRI time series. Let $\boldsymbol{y}_{ivt}$ represent the blood oxygenation level-dependent (BOLD) signals from fMRI. The scalar value of covariate j for $j = 1, ..., J$ at time t is denoted by x_{ijt}. Define $\boldsymbol{x}_{it} \in R^J = [\boldsymbol{x}_{i1t}, \boldsymbol{x}_{i2t}, \ldots, \boldsymbol{x}_{iJt}]^T$ as covariates at time t, where $\boldsymbol{x}_{i1t}$ and $\boldsymbol{x}_{i2t}$ are the eye-blink and eye-fixation covariates of interest, $\boldsymbol{x}_{i3t}, \ldots, \boldsymbol{x}_{iJt}$ are nuisance covariates controlling for motion artifacts. These covariates remain constant across different brain regions. Let $\boldsymbol{\beta}_{iv}$ denote the subject-level coefficient matrix. Let $\boldsymbol{e}_{ivt}$ denote the error term.

3.2 Task activation model

3.2.1 Mean model: Autoregressive modeling of regional neural dynamics

At the single-subject level, define the first-level model as follows:

$$\boldsymbol{y}_{ivt} = \boldsymbol{x}_{it}^T \boldsymbol{\beta}_{iv} + \boldsymbol{e}_{ivt}, \tag{1}$$

where $\boldsymbol{e}_{iv} \sim \mathcal{N}(0, \boldsymbol{\xi}_{iv}^2 \boldsymbol{\Psi}_{iv})$ with $\boldsymbol{e}_{iv} = [\boldsymbol{e}_{iv1}, \ldots, \boldsymbol{e}_{ivT}]^T$, $\boldsymbol{\xi}_{iv}^2$ is the variance, which is constant across time, and $\boldsymbol{\Psi}_{iv}$ captures autocorrelation. There is empirical support for the use of a stationary autoregressive (AR) model for the errors in Equation (1) (Worsley et al., 2002). Further investigations have determined that an AR(3) model is preferred in many locations within a task-based fMRI context (Mejia et al., 2019). Consequently, we applied an AR(3) model across all brain regions.

Let B denote the back-shift operator, where $B^l * y_{ivt} = y_{iv,t-l}$. The AR(3) model is

$$(1 - \phi_{iv1}B - \phi_{iv2}B^2 - \phi_{iv3}B^3)(\boldsymbol{y}_{ivt} - \boldsymbol{x}_{it}^T \boldsymbol{\beta}_{iv}) = \boldsymbol{\epsilon}_{ivt}, \tag{2}$$

where $\boldsymbol{\epsilon}_{ivt} \overset{\text{i.i.d.}}{\sim} N(0, \tau_{iv}^2)$. Equation (2) indicates that $\boldsymbol{\epsilon}_{ivt}$ are independent and identically distributed errors with innovation variance τ_{iv}^2. This contrasts with $\boldsymbol{e}_{ivt}$ in Equation (1), which are the correlated errors. In our dynamic connectivity analysis in Section 3.3.1, we will model the spatial covariance structure of $\boldsymbol{\epsilon}_{ivt}$ across regions $v = 1, \ldots, V$. We employed the 'ARIMA' function (Ripley, 2002) from the 'stats' package (R Core Team, 2024), included in the base R environment, to fit the AR(3) modelEquation (2).

3.2.2 Population-level Effects

To quantify the population-level effects on brain activation in response to eye-blink and eye-fixation events, we used the general linear model for fMRI task activation, which is a hierarchical model with population slopes and subject deviations (Friston et al., 1994). Let A_i denote the presence of ASD, with $A_i = 1$ for ASD participants and $A_i = 0$ for non-ASD participants. We defined three parameters for the group-stage analysis:

$$\boldsymbol{\beta}_{iv1} = \alpha_{v1} + \gamma_{v1} A_i + \nu_{iv1}, \quad \text{(Model 1)} \tag{3}$$

$$\boldsymbol{\beta}_{iv2} = \alpha_{v2} + \gamma_{v2} A_i + \nu_{iv2}, \quad \text{(Model 2)} \tag{4}$$

$$\boldsymbol{\beta}_{iv2} - \boldsymbol{\beta}_{iv1} = (\alpha_{v2} - \alpha_{v1}) + (\gamma_{v2} - \gamma_{v1}) A_i + (\nu_{iv2} - \nu_{iv1}). \quad \text{(Model 3)} \tag{5}$$

In the hierarchical formulation, $\boldsymbol{\beta}_{iv1}$ is the subject-specific slope from Equation (2) for eye-blink, which equals the population slope of eye-blink, α_{v1}, plus the population-modification of this slope by ASD, γ_{v1}, plus random subject slopes, ν_{iv1}. These values are similarly defined for eye-fixation in Model 2. Model 3 captures the contrast between eye-fixation and eye-blink. Since people blink less when they are paying attention, the contrast between eye-fixation and eye-blink events contains information on engagement. This contrast also captures physiological processes that differ between eye-fixation and eye-blink events. These

physiological processes are generally of less interest than engagement, but still of potential use in understanding brain activity.

To estimate α_{v1} and γ_{v1} in Model 1, we began by acquiring the estimated $\hat{\boldsymbol{\beta}}_{iv1}$ from the AR(3) model, as specified in Equation (2), for each participant across all V brain regions. Subsequently, we fitted a general linear model to these $\hat{\boldsymbol{\beta}}_{iv1}$ estimates, incorporating the indicator variable A_i. The methodology for Models 2 and Model 3 followed a similar procedure.

3.3 Dynamic functional connectivity

3.3.1 Covariance regression model

To quantify the relationship between dynamic functional connectivity and eye-tracking events, we proposed the below covariance regression model at the single-subject level:

$$\boldsymbol{\Sigma}_{it} = \mathbf{Cov}(\boldsymbol{\epsilon}_{it}|\boldsymbol{x}_{it}) = \boldsymbol{B}_{i0} + \sum_{j=1,..,J} \boldsymbol{B}_{ij} x_{ijt}, \tag{6}$$

where $\boldsymbol{\Sigma}_{it}$ denotes the time-varying $V \times V$ covariance matrix, reflecting the task-based dynamic connectivity; $\boldsymbol{\epsilon}_{it}$ denote the $V \times 1$ vector of residuals at time point t, derived from the mean model as detailed in Equation (2). Specifically,

- The term $\boldsymbol{B}_{i0}$ captures the static functional connectivity between pairs of brain regions, represented as a time-invariant $V \times V$ matrix.
- $\boldsymbol{B}_{ij}$, $j = 1, \ldots, J$, denotes a symmetric $V \times V$ matrix of the effect of task and nuisance covariates on the conditional covariance, remaining constant over time.
- $\boldsymbol{\eta}_{it}$ is defined as a $V \times V$ matrix of residuals, capturing the variation not explained by the conditional covariance model.

From the covariance regression model, the estimated matrices $\hat{\boldsymbol{B}}_{ij}, j = 1, \ldots, J$ can be used to interpret the dynamic functional connectivity in response to task predictors and nuisance covariates. Specifically for this study, $\hat{\boldsymbol{B}}_{i1}$ represents the influence of eye-blink, while $\hat{\boldsymbol{B}}_{i2}$ corresponds to the impact of eye-fixation on the changing patterns of dynamic brain functional connectivity. Let $\hat{\boldsymbol{b}}_{ij(vv')}$ represent the estimated effect within the vv' cell of $\hat{\boldsymbol{B}}_{ij}$. The estimation process for these estimators is detailed in Section 3.3.2.

3.3.2 Estimation using Least Squares

We propose to use univariate Ordinary Least Squares (OLS) to estimate the parameters in (6) for each edge (vv'). Analytically, we first obtained a $V \times V \times T$ array by constructing:

$$\widehat{\mathbf{Cov}}(\hat{\boldsymbol{\epsilon}_{it}}) = \hat{\boldsymbol{\epsilon}}_{it}\hat{\boldsymbol{\epsilon}}_{it}^T \tag{7}$$

where $\hat{\boldsymbol{\epsilon}}_{it}$ is residuals from Equation (2).

To obtain the estimations, define $\widehat{\mathbf{Cov}}(\hat{\boldsymbol{\epsilon}}_i)_{vv'} = [\hat{\boldsymbol{\epsilon}}_{iv1}\hat{\boldsymbol{\epsilon}}_{iv'1}, \hat{\boldsymbol{\epsilon}}_{iv2}\hat{\boldsymbol{\epsilon}}_{iv'2}, \ldots, \hat{\boldsymbol{\epsilon}}_{ivT}\hat{\boldsymbol{\epsilon}}_{iv'T}]^T$ as $T \times 1$ vector for region pair vv', derived from Equation (7). Let $X_i = [\mathbf{1}^T, \boldsymbol{x}_{i1}^T, \boldsymbol{x}_{i2}^T, ..., \boldsymbol{x}_{iJ}^T]$, a

$T \times (J+1)$ matrix, denote the design matrix. There are total $\frac{V(V+1)}{2}$ OLS regression models for a single subject with V brain regions. Let $\tilde{\boldsymbol{\eta}}_{it(vv')}$ denote the error component corresponding to the vv' edge in $\boldsymbol{\eta}_{it}$. Consequently, each edge's estimated effects $\hat{\boldsymbol{b}}_{i(vv')}$ and residuals $\tilde{\boldsymbol{\eta}}_{i(vv')}$ can be obtained from their respective OLS models:

$$\hat{\boldsymbol{b}}_{i(vv')} = \left(X_i^T X_i\right)^{-1} X_i^T \widehat{\mathbf{Cov}}(\hat{\boldsymbol{\epsilon}}_i)_{vv'}, \tag{8}$$

$$\tilde{\boldsymbol{\eta}}_{i(vv')} = X_i \hat{\boldsymbol{b}}_{i(vv')} - \widehat{\mathbf{Cov}}(\hat{\boldsymbol{\epsilon}}_i)_{vv'}, \tag{9}$$

In Section 3.4, we apply the log-Euclidean transformation to $V \times V \times T$ array constructed in Equation (7), resulting in the updated forms of Equation (8) and Equation (9). Further, in Section 4.4.1, we employ $\tilde{\boldsymbol{\eta}}_{it(vv')}$ from Equation 9 to conduct model diagnostics.

3.3.3 Statistical considerations in the covariance regression model

At the individual level, we calculated Z-statistics to measure the differential estimated effects of eye-fixation ($\hat{\boldsymbol{B}}_{i2}$) versus eye-blink ($\hat{\boldsymbol{B}}_{i1}$) described in Section 3.3.1. Consequently, the $V \times V$ Z-statistics matrix $\boldsymbol{Z}_i$ reflects the distinct effects of eye-fixation in contrast to eye-blink on the brain's dynamic functional connectivity.

Let $\boldsymbol{Z}_{i,(vv')}$ denote the Z-statistics for vv' region. For a single edge vv':

$$\boldsymbol{Z}_{i,(vv')} = \frac{\hat{\boldsymbol{B}}_{i2,(vv')} - \hat{\boldsymbol{B}}_{i1,(vv')}}{\sqrt{\widehat{\mathrm{Var}}(\hat{\boldsymbol{B}}_{i2,(vv')}) + \widehat{\mathrm{Var}}(\hat{\boldsymbol{B}}_{i1,(vv')}) - 2 \cdot \widehat{\mathrm{Cov}}(\hat{\boldsymbol{B}}_{i2,(vv')}, \hat{\boldsymbol{B}}_{i1,(vv')})}} \tag{10}$$

A positive value in $\boldsymbol{Z}_{i,(vv')}$ indicates a stronger influence from eye-fixation, whereas a negative value suggests that eye-blink has a more substantial effect on the evolving covariance pattern. In other words, a positive value signifies that engagement events have a greater impact on brain dynamic functional connectivity. For each participant and each edge, we generated the subject-specific $V \times V$ $Z_{i,\hat{\boldsymbol{B}}_{i2}-\hat{\boldsymbol{B}}_{i1}}$ matrices based on Equation (10). These matrices will be extensively presented and discussed in Section 5.3.

3.3.4 Population-level effects

To quantify the population effects in $V \times V$ matrices $\boldsymbol{Z}_{i,\hat{\boldsymbol{B}}_{i2}-\hat{\boldsymbol{B}}_{i1}}$ between ASD and non-ASD group, we applied the following linear model for each edge to assess the difference in Z-statistics between eye-fixation versus eye-blink effects in two groups.

Let $\boldsymbol{Z}_{i,(vv')}$ denote the Z-statistics for a single vv' region:

$$E(\boldsymbol{Z}_{i,(vv')}) = \boldsymbol{\rho}_{i0,(vv')} + \boldsymbol{\rho}_{i1,(vv')} A_i \tag{11}$$

Here, $\boldsymbol{\rho}_{i0,(vv')}$ denotes the population effects on edge vv', while $\boldsymbol{\rho}_{i1,(vv')}$ indivates the effects modifications within ASD group. Ultimately, we derived a $V \times V$ matrix for the mean Z-statistics in the non-ASD group ($\bar{\boldsymbol{Z}}_{\text{non-ASD}}$) and for the effects modifications in participants of the ASD group ($\bar{\boldsymbol{Z}}_{\text{ASD}}$). The results of the visualization of these two matrices will be shown in Section 5.3.2.

3.4 Log-Euclidean transformation

We utilized a log-Euclidean framework, akin to working with log-transformed univariate responses (Schwartzman, 2016) on Equation (7). To obtain the log-Euclidean transformed form, we first conducted the eigenvalue decomposition on $\mathbf{Cov}(\hat{\boldsymbol{\epsilon}}_{it})$ as follows: $\mathbf{Cov}(\hat{\boldsymbol{\epsilon}}_{it}) = \boldsymbol{U}_{it}\boldsymbol{\Lambda}_{it}\boldsymbol{U}_{it}^T$. Here, $\boldsymbol{U}_{it}$ is the matrix of eigenvectors, and $\boldsymbol{\Lambda}_{it}$ is a diagonal matrix comprising only one non-negative eigenvalues of $\boldsymbol{\Sigma}_{it}$. We retain only the non-negative eigenvalue, setting all other eigenvalues to 0. By taking the logarithm of $\boldsymbol{\Lambda}_{it}$, denoted as $\log \boldsymbol{\Lambda}_{it}$, we reformulate the model in the log space, where the covariance structure can be expressed in terms of the log-transformed variables:

$$\log \widehat{\mathbf{Cov}}(\hat{\boldsymbol{\epsilon}}_{it}) = \log(\hat{\boldsymbol{\epsilon}}_{it}\hat{\boldsymbol{\epsilon}}_{it}^T) = \boldsymbol{U}_{it} \log \boldsymbol{\Lambda}_{it}\boldsymbol{U}_{it}^T$$

This logarithmic representation ensures that the covariates remain within the space of symmetric matrices, and the results obtained can subsequently be back-transformed to the original scale. In this framework, the log transformed forms of Equation (8) and Equation (9) can be updated to as follows:

$$\hat{\boldsymbol{b}}^*_{i(vv')} = \left(X_i^T X_i\right)^{-1} X_i^T \log \widehat{\mathbf{Cov}}(\hat{\boldsymbol{\epsilon}}_i)_{vv'}, \tag{12}$$

$$\tilde{\boldsymbol{\eta}}^*_{i(vv')} = X_i \hat{\boldsymbol{b}}^*_{i(vv')} - \log \widehat{\mathbf{Cov}}(\hat{\boldsymbol{\epsilon}}_i)_{vv'}, \tag{13}$$

We investigated both the untransformed (Equations 8 and 9) and log-transformed (Equations 12 and 13) versions of the model, focusing particularly on addressing heteroscedasticity issues in Section 3.5 and verifying normality assumptions in Section 4.4.1.

3.5 Robust estimation

Within the Ordinary Least Squares (OLS) estimation framework, the residuals $\tilde{\boldsymbol{\eta}}_{it(vv')}$ in Equation Equation (9) and $\tilde{\boldsymbol{\eta}}^*_{it(vv')}$ from Equation Equation (13) are assumed to be independent, satisfying the assumptions of homoscedasticity, linearity, and normality.

To address the potential heteroscedasticity issue, and ensure an accurate statistical inference process, we employed a heteroscedasticity consistent covariance matrix estimation (Long and Ervin, 2000). For each vv'':

$$\widehat{Cov}(\hat{\boldsymbol{b}}_{i,(vv')}) = (X_i'X_i)^{-1}X_i'\boldsymbol{D}_i X_i (X_i'X_i)^{-1}.$$

$\boldsymbol{D}_i$ is the diagonal matrix in which each diagonal element is $\frac{\tilde{\eta}^2_{i,(vv'),t}}{(1-h_{i,tt})^2}$, where $h_{i,tt}$ is the t^{th} diagonal element of the hat matrix $X_i(X_i'X_i)^{-1}X_i'$ and $\tilde{\eta}_{i,(vv'),t}$ is the residual from Equation (9). The similar approach was employed to log-Euclidean transformed forms described in Section 3.5 and the residual from Equation (13). This robust estimation approach effectively mitigates heteroscedasticity, ensuring reliable inference for $\hat{\boldsymbol{B}}_{ij}$.

4 Data processing and analysis

4.1 Overview of estimation steps

1. **Eye-tracking Data Processing**: We performed the convolution of eye-blink and eye-fixation signals with the Hemodynamic Response Function (HRF). This step involves aligning the sampling rates in the eye-tracking convolution data with the fMRI time series.

2. **fMRI Time Series Processing**: We adopted the Schaefer 100 parcellation scheme (Schaefer et al., 2018) in this thesis. This approach divides the cerebral cortex into 100 regions, and each region is labeled with one of seventeen functional networks. The Schaefer100 parcels are accessible for use within the R package ciftiTools (Pham et al., 2022).

3. **Autoregressive modeling**: We applied the AR(3) model, as detailed in Section 3.2.1, to examine fMRI time series data across 100 brain regions for each participant. This analysis estimated the region-specific impacts of eye-blink and eye-fixation events on brain activation using the 'ARIMA' function (Ripley, 2002) in the base R environment, producing residuals unique to each region.

4. **Log-Euclidean Transformation**: We applied the log-Euclidean transformation to the $V \times V \times T$ array as discussed in Section 3.4, which constructs the $T \times 5050$ response matrix for least squares analysis.

5. **Least Squares Regression**: We estimated the coefficient matrices, $\hat{\boldsymbol{B}}_{i1}$ and $\hat{\boldsymbol{B}}_{i2}$, by fitting 5050 linear models, then estimated the standard errors for the coefficients using the heteroscedastic consistent errors (see Section 3.5).

4.2 Processing the eye-tracking data

4.2.1 Convolution of eye-tracking events with the HRF function

During two movie-watching tasks, we recorded eye-blink and eye-fixation events for each participant. We extracted onset times and durations from the eye-tracking raw data, with onset times marking the start of each event and durations indicating their length. By leveraging the onset, duration, sampling rate (500 Hz), and the overall task duration, we constructed boxcar functions for both eye-blink and eye-fixation events within each task. Subsequently, we performed convolution (Zumer et al., 2010) of these eye-tracking events with the Double-gamma Hemodynamic Response Function (HRF) (Welvaert et al., 2011). This process generated the BOLD signals corresponding to eye-blink ($j = 1$) and eye-fixation ($j = 2$), which served as the two task predictors and main effects in this study.

Let $\boldsymbol{f}$ denote the time series of the eye-tracking onset boxcar function and let $\boldsymbol{h}$ denote the HRF,

$$(h * f)_t = \int_0^t h(\tau) f(t - \tau)\, d\tau.$$

We employed Fast Fourier Transform (FFT) techniques to make the convolution process computationally efficient.

$$\text{Convolution Operation in Frequency Domain: } S_{\text{conv}}(f) = \mathcal{F}\{s(t)\} \cdot \mathcal{F}\{\text{hrf}(t)\}$$

$$\text{Resulting Convolved Signal in Time Domain: } s_{\text{conv}}(t) = \Re\left\{\mathcal{F}^{-1}\{S_{\text{conv}}(f)\}\right\} \times \frac{1}{N}$$

where $\mathcal{F}$ denotes the Fourier transform, $\mathcal{F}^{-1}$ represents the inverse Fourier transform, N is the normalization factor corresponding to the number of eye-tracking data points, and $\Re$ indicates the real part of the complex inverse Fourier transform result.

4.2.2 Alignment with fMRI Time Series

Eye-tracking data were collected at a sampling rate of 500 Hz, resulting in a total of $T \times 500$ data points for each task. To match the convolved time series of eye-tracking events with the sampling rate of the fMRI time series, we extracted the time points of the convolved data points that corresponding to the sampling time points of the fMRI acquisition (every 1.127 seconds, with a precision of +/- 0.001 seconds), generating the T-length time series for the convolved signals. Subsequently, we normalized these time series so that the peak value of the convolution signals reached 1, denoted as $\boldsymbol{x}_{i1}$ and $\boldsymbol{x}_{i2}$ for eye-blink and eye-fixation events, respectively.

Figure 1: Convolution of Eye-Tracking Metrics with the HRF Function for a Single Subject. These signals are later used as predictors in the general linear model of fMRI task activation **Top**: Eye-blinking. **Bottom**: Eye-fixation.

Figure 1 illustrates an example of one subject's standardized convolved HRF and eye-blink (top) and eye-fixation (bottom) events during movie-watching task 1. The blue lines depict the standardized convolved signals for eye-tracking events, while the orange vertical lines mark the boxcar function for eye-tracking events. The green boxes at the top of the figure represent the sequence comprising a three-second crosshair, three video clips interspersed with 15-second crosshairs, and ending with a 12-second crosshair for validation.

4.3 Task activation analysis

4.3.1 Model covariates

In addition to the two eye-blink and eye-fixation convolved signals ($\boldsymbol{x}_{i1}, \boldsymbol{x}_{i2}$) presented in 4.2, our model included six motion parameters—translational movements along the x, y, and z axes (*trans_x*, *trans_y*, *trans_z*) and rotational movements around the x, y, and z axes (*rot_x*, *rot_y*, *rot_z*)—and the quadratic terms of these head movement parameters as covariates ($\boldsymbol{x}_{i3}, ...\boldsymbol{x}_{i,14}$). These covariates help control for potential confounding effects due

to head motion during the fMRI scanning process. Additionally, we utilized an indicator variable $\boldsymbol{x}_{i,15}$ to differentiate between the two task sessions, with an indicator value of 1 for movie-watching task two and 0 for task one. The index of time points (from 1 to T) and a quadratic term of the time index ($\boldsymbol{x}_{i,16}, \boldsymbol{x}_{i,17}$) were also included in our model to account for possible scanner drift. Additionally, to account for the varying effects of these covariates across different task sessions, we introduced 14 interaction terms $\boldsymbol{x}_{i,18}, ..., \boldsymbol{x}_{i,31}$ (interaction between task session indicator and the other nuisance variables, i.e., the 12 head motion parameters and the 2 time variables).

All covariates were standardized except for $\boldsymbol{x}_{i1}$ and $\boldsymbol{x}_{i2}$. This was done to optimize the parameter estimation process in the ARIMA function (Ripley, 2002) in R, which utilizes general-purpose optimization and tends to perform best when regressors are centered around zero mean and scaled to unit variance. Consequently, these 31 covariates constituted the design matrix in the final model.

4.3.2 Single subject autoregressive modeling process

Using 31 covariates, we fit the AR(3) model in Equation (2) for each of the 100 brain regions separately for each subject. The effectiveness of the AR(3) model was validated by examining the Autocorrelation Function (ACF) and Partial Autocorrelation Function (PACF) plots of the residuals.

To evaluate potential multicollinearity between eye-blink and eye-fixation events, we revisited the linear model using the same covariates set and examined the variance inflation factor (VIF) values. The results showed no significant multicollinearity issues, with VIF values around 1.5 for the convolved eye-blink and eye-fixation signals across all subjects.

4.3.3 Population-level effects

To quantify the population effects in ASD and non-ASD, we applied the three linear models as detailed in Section 3.2.2. The $\hat{\boldsymbol{\beta}}_{iv1}$ and $\hat{\boldsymbol{\beta}}_{iv2}$ were estimated form Equation (2). As a result, we obtained $\hat{\gamma}_{v1}$, $\hat{\gamma}_{v2}$, $\hat{\alpha}_{v1}$, and $\hat{\alpha}_{v2}$, respectively. Specifically, $\hat{\alpha}_{v1}$ and $\hat{\alpha}_{v2}$ represent the global population effects of eye-blink and eye-fixation on brain activity. $\hat{\gamma}_{v1}$ and $\hat{\gamma}_{v2}$ quantify how the eye-blink and eye-fixation effects differ from the global population effects, respectively. These estimators are visualized and detailed in Section 5.2.

4.4 Covariance regression modeling process

For each individual, we utilized the same set of $J = 31$ covariates as in the AR(3) model to model the covariance of residuals, $\hat{\boldsymbol{\epsilon}}_{it} \cdot \hat{\boldsymbol{\epsilon}}_{it}^T$, a $100 \times 100 \times T$ array, where the $\hat{\boldsymbol{\epsilon}}_{it}$ were derived from the 100's AR(3) models in Equation (2). Additionally, for each OLS model, an updated $T \times (31 + 1)$ design matrix $X_i = [\mathbf{1}^T, \boldsymbol{x}_{i1}^T, \boldsymbol{x}_{i2}^T, ..., \boldsymbol{x}_{iJ}^T]$ were constructed for each participant.

Next, $\frac{V \cdot (V+1)}{2} = \frac{100 \cdot (101)}{2} = 5050$ OLS models were fitted to examine the dynamics of functional connectivity $\widehat{\mathbf{Cov}}(\hat{\boldsymbol{\epsilon}}_{it})$ within the brain for each individual. We applied both the untransformed $\widehat{\mathbf{Cov}}(\hat{\boldsymbol{\epsilon}}_{it})$ and the log-Euclidean transformation $\log\widehat{\mathbf{Cov}}(\hat{\boldsymbol{\epsilon}}_{it})$ methods as detailed in Section 3.4. A comprehensive comparison of these two approaches (untransformed vs. log-Euclidean transformation) and their diagnostics is presented in the following section.

4.4.1 Comparison between untransformed vs. log-transformed

We examined the residuals for both untransformed ($\tilde{\boldsymbol{\eta}}_{i,(vv')}$) and log-Euclidean transformed ($\tilde{\boldsymbol{\eta}}^{*}_{i,(vv')}$) methods. Extensive diagnostics on randomly chosen brain region pairs indicate the log-Euclidean transformation improves normality. For illustration purposes, we depict 4 brain region pairs (vv') from 4 randomly selected participants (2 ASD and 2 non-ASD). Figure 2 presents a comparison of residuals before and after the application of the log-Euclidean transformation.

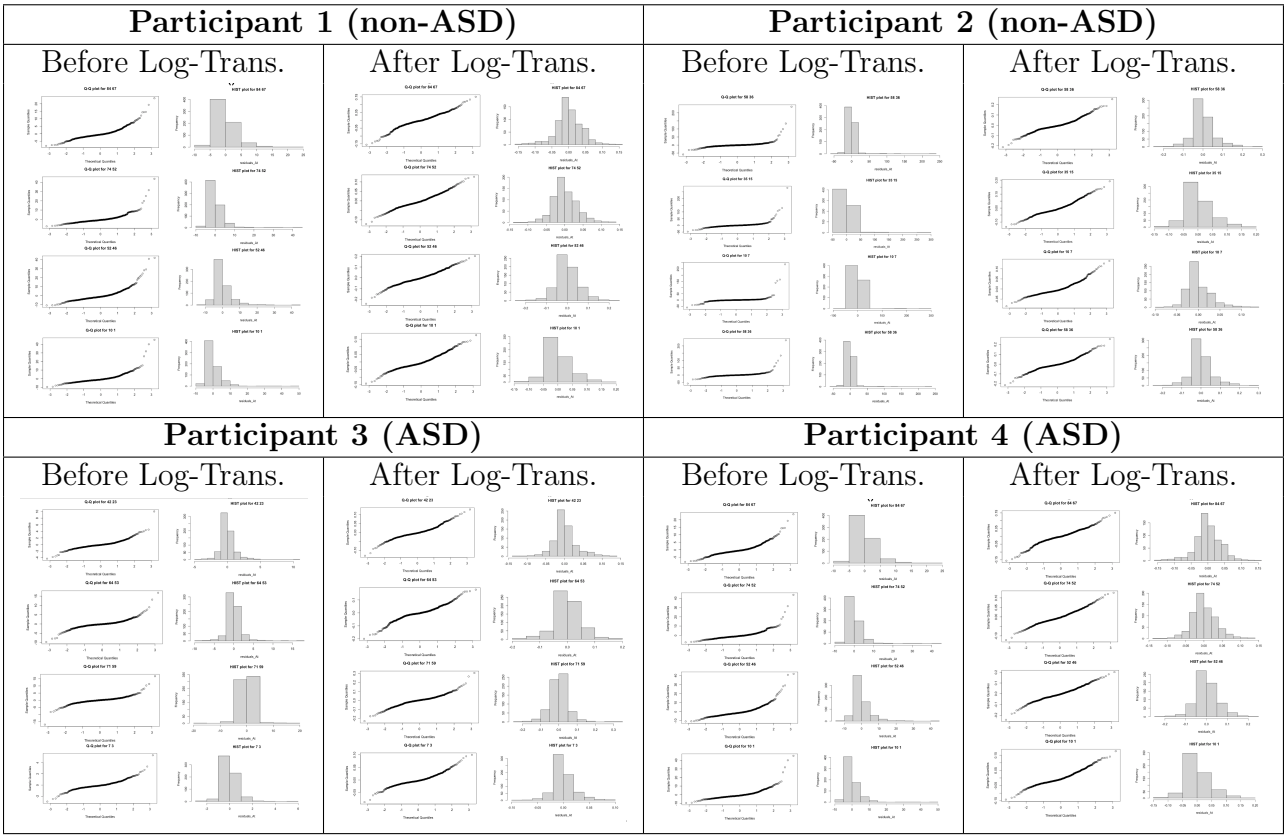

Figure 2: Quantile-Quantile (Q-Q) Plot Analysis for OLS Model Residuals was conducted on brain region pairs vv', which were randomly selected from two participants diagnosed with Autism Spectrum Disorder (ASD) and two Typically Developing (non-ASD) participants, with the pairs themselves also chosen at random.

Prior to log-transformation, the Q-Q plots for participants exhibit deviations from the line of normality, particularly with a skewness that suggests a non-normal distribution of the residuals in both ASD and non-ASD participants' brain region pairs (Figure 2).

After the log-transformation, the Q-Q plots align more closely with the line of normality, indicating that the transformation reduces skewness. Thus, we use the log-Euclidean transformation. To further address deviations from normality, we use heteroscedasticity consistent standard errors for inference as described in Section 3.5.

4.5 Assessment of autocorrelation

To evaluate possible autocorrelation concerns on covariance regression, we analyzed the residuals ($\tilde{\boldsymbol{\eta}}_i^*$) from 5050 OLS models with ACF and PACF plots. These diagnostics showed no significant autocorrelation issues within the OLS framework, as autocorrelation for initial lags remained within acceptable threshold.

4.5.1 Covariance estimation

We derived $V \times V$ matrices of coefficients $\hat{\boldsymbol{B}}_{ij}, j = 1, 2, ..., 32$ for each participant through the 5050 OLS models. These estimated $V \times V$ matrices capture the influence of the task predictors and other nuisance covariates on brain functional connectivity over time in a linear fashion. Particularly, this study focused on $\hat{\boldsymbol{B}}_{i1}$ and $\hat{\boldsymbol{B}}_{i2}$, which represent the effects of eye-blink and eye-fixation on dynamics of functional connectivity, respectively.

Finally, to compare the association between brain dynamic of functional connectivity and eye-tracking events. We derived the subject-specific $V \times V$ Z_i matrices based on Equation (10) for each participant. These matrices will be presented and discussed in Section 5.3.

5 Results

5.1 Summary statistics of eye movement measurements

The exploration of raw eye-tracking data for current data cohort reveals distinct patterns in the visual engagement of participants (Table 1). Females with ASD demonstrated a decline in median eye-fixation percentages, from 85.56% (Q1: 83.98, Q3: 87.13) in the initial video of Movie 1 (0021 SAND) to 64.58% (Q1: 59.12, Q3: 77.46) by the final video of Movie 2 (0025 DOLL), suggesting a potential decrease in attention to the visual stimuli as the task progressed. Conversely, ASD males, while exhibiting an overall decline, maintained a relatively higher eye-fixation percentage throughout the series of videos compared to female participants.

Conversely, non-ASD participants showed more consistent eye-fixation percentages across the duration of the task. Non-ASD females consistently had slightly higher eye-fixation percentages than non-ASD males, with numbers displaying minimal variation—from 90.43% (Q1: 88.41, Q3: 93.75) in the first video clip to 90.15% (Q1: 83.31, Q3: 91.50) by the fifth video clip for females, and from 89.46% (Q1: 87.38, Q3: 92.35) to 88.45% (Q1: 86.06, Q3: 89.79) for males. This points to a stable level of visual attention throughout the session.

The summary of median eye-blink percentages revealed that ASD females exhibited an increase in eye-blink rates, increasing from 2.81% (Q1: 2.59, Q3: 3.03) in the initial video to 19.91% (Q1: 10.98, Q3: 30.47) by the final video, suggesting a decrease in visual task engagement over time. Conversely, ASD males showed lower median eye-blink percentages, reflecting less frequent blinking during the tasks. In contrast, non-ASD children, regardless of sex, maintained stable eye-blink rates across the videos, indicating a consistent level of visual attention.

The observed patterns reveal differences in attentional engagement among ASD and non-ASD groups. ASD individuals, particularly females, demonstrate decreasing attention over time in prolonged visual tasks. Meanwhile, non-ASD children maintain consistent attention levels, highlighted by stable eye-tracking measurements. An interesting point is the reduced fixation percentages in videos 0023 DOLL and 0022 SAND across all participants, possibly due to the segments' less engaging visual content.

These preliminary findings are based on a limited sample size, currently comprising only four females in the ASD group, and may be subject to change as more data are collected.

5.2 Group-level analysis: Eye-fixation and eye-blink Effects

5.2.1 Mean effects of non-ASD group : $\hat{\alpha}_{v1},\ \hat{\alpha}_{v2},\ \hat{\alpha}_{v2} - \hat{\alpha}_{v1}$

Figure 3 presents a series of brain activation maps based on analyses from three linear models as outlined in Section 3.2.2, mapping out the brain's activation associated with eye-blink and eye-fixation events within non-ASD cohort. The left column reveals baseline brain activation impacts across 100 regions due to eye-blink events (Model 1) and eye-fixation events (Model 2), alongside the comparative impacts between eye-fixation and eye-blink events (Model 3). The intensity of colors on these maps signifies the magnitude of effects, showcasing the regions activated by each eye movement type. The middle and right columns highlight the brain regions surpassing the False Discovery Rate (FDR) adjusted p-value significance levels of 0.05 and 0.2, visualized using $-\log_{10}$(FDR-adjusted p-value).

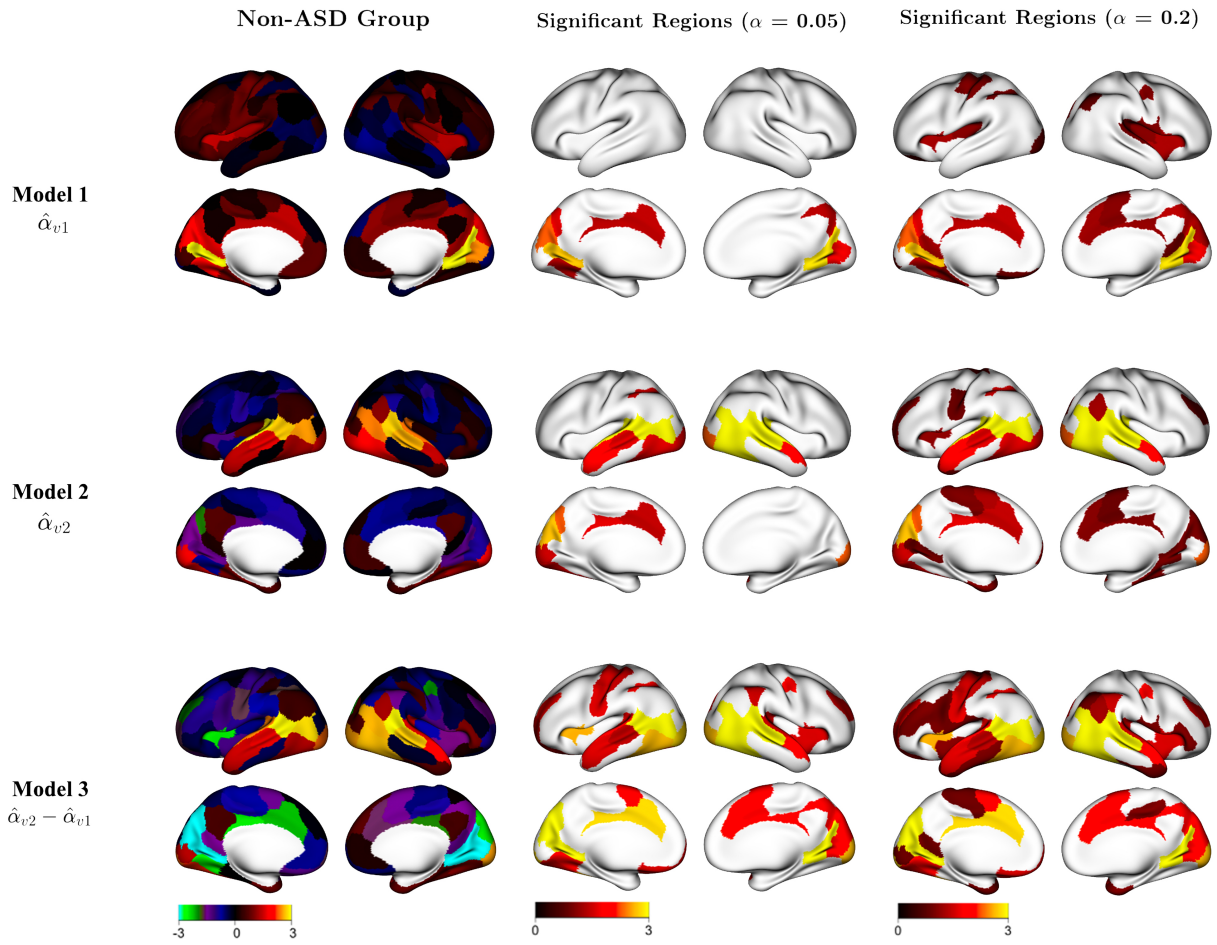

Figure 3: **Left:** Global brain activation (Mean effects in non-ASD group) from three models for 100 brain regions, representing the effects of eye-blink, eye-fixation, and the differential effects between eye-fixation and eye-blink. **Middle:** Brain regions surpassing the False Discovery Rate (FDR) adjusted p-value threshold of 0.05. **Right:** Brain regions surpassing the FDR adjusted p-value threshold of 0.2.

Figure 3 revealed distinct patterns in the association between brain activity and eye-blink and eye-fixation events while watching movies. When applying a significance level adjusted for false discovery rate (FDR) of 0.05, we found that eye-blink events were significantly associated with the brain activation in right hemisphere's (RH) Default Mode Network C, Visual Area B, and the left hemisphere's (LH) Salience/Ventral Attention Network A and Control Network C.

Eye-fixation events, on the other hand, showed a strong association with brain activity in different areas, including the RH Visual Cortex A, Visual Cortex C, as well as both hemispheres' Salience/Ventral Attention, Default Mode, Control, and Dorsal Attention Networks, and Language Processing Areas.

Furthermore, we observed significant differences in the association between brain activation with eye-fixation compared to eye-blink events during the movie-watching tasks. Notably, the LH Auditory cortex, Visual Areas A & B, part of the Dorsal Attention Network, Salience/Ventral Attention Network A, and Control Network C responded differently

to eye-fixation compared to eye-blink events. In the right hemisphere, the Default Mode Network C, Visual Areas A and B, Salience/Ventral Attention Networks A and B, and Language Processing Areas showed varied brain activation during these visual tasks.

5.2.2 Mean differential effects in ASD vs. non-ASD group : $\hat{\gamma}_{v1}$, $\hat{\gamma}_{v2}$, $\hat{\gamma}_{v2} - \hat{\gamma}_{v1}$

Figure 4 depicts how brain activation patterns differ between ASD and non-ASD children during eye-tracking events. (estimated coefficients of A_i described in Section Section 3.2.2). Specifically, it visualizes the contrasting brain activation responses to blinking events (Model 1), eye fixation events (Model 2) in the ASD group compared to the non-ASD group. Additionally, it highlights the difference in brain activation in response to eye-fixation versus eye-blink in ASD compared to non-ASD children (Model 3). Regions with significantly altered activity at a false discovery rate of 0.2 are shown in the right column through the visualization of $-\log_{10}$(FDR-adjusted p-value).

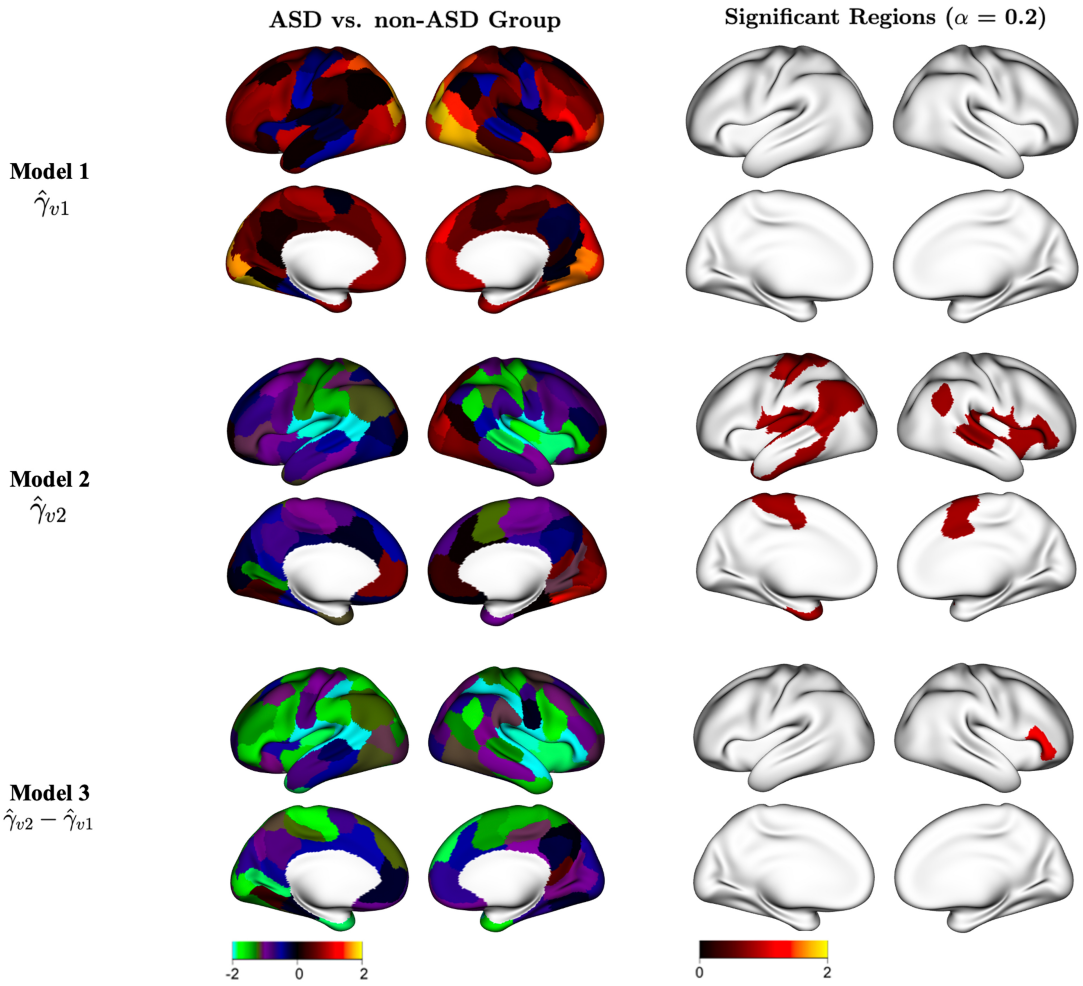

Figure 4: **Left:** Mean differential effects modifications in ASD versus non-ASD in brain activation during eye-blink events, eye-fixation events, and when comparing the effects during eye-fixation versus eye-blink events. **Right:** Brain regions selected using an FDR adjusted p-value threshold of 0.2.

At a significance threshold of 0.2, brain activations during eye-blink events did not show significant differences between ASD and non-ASD participants. However, the study identified several brain regions in the ASD group that exhibited significantly different activation during eye-fixation events compared to the non-ASD group. Notably, the LH Somatomotor Areas A and B, Default Mode Network B, Auditory Cortex, and Control Network B, along with the RH Salience/Ventral Attention Network A, Default Mode Network A, Language Processing Areas, Salience/Ventral Attention Network B, and Somatomotor Area B, demonstrated distinctive activation during eye-fixation events. Importantly, all of these significant regions have negative coefficients, indicating decreased brain activation during eye-fixation events among ASD participants.

Moreover, a comparison of brain activation during eye-fixation versus eye-blink events between ASD and non-ASD groups revealed that only the right hemisphere Language Processing Area showed a significant difference, with the observed value being negative. This

suggests that the right hemisphere Language Processing Area in ASD participants had a smaller difference in activation between eye-fixation and eye-blink events than in the non-ASD group. Essentially, brain activation in ASD participants was more similar for eye-fixation and eye-blink events compared to that of non-ASD participants. This implies that the Language Processing Area exhibits lower sensitivity to engagement in individuals with ASD compared to those without ASD.

Additionally, the majority of brain regions in Model 2 and all regions in Model 3 exhibit negative values, suggesting reduced brain activation in the ASD group relative to the non-ASD group during eye-fixation. Moreover, Model 3 reveals that the contrasts between eye-fixation and eye-blink activation is generally smaller in the ASD group compared to the non-ASD group. This could imply that the differences in brain activation associated with eye-fixation and eye-blink are less distinct in individuals with ASD.

5.3 Covariance Regression Modeling

5.3.1 Single-subject associations between dynamic functional connectivity and eye-tracking events

To understand individual patterns of brain dynamic functional connectivity obtained through covariance regression, as discussed in Section 3.3.1, we randomly selected three participants diagnosed with ASD and three non-ASD participants for visualization. Heatmap plots were used to display the estimated linear associations of eye-tracking events on brain dynamic functional connectivity patterns. Figure 5 presents these heatmap plots, visualizing the Z-statistics ($\boldsymbol{Z}_i$) as detailed in Section 3.3.3.

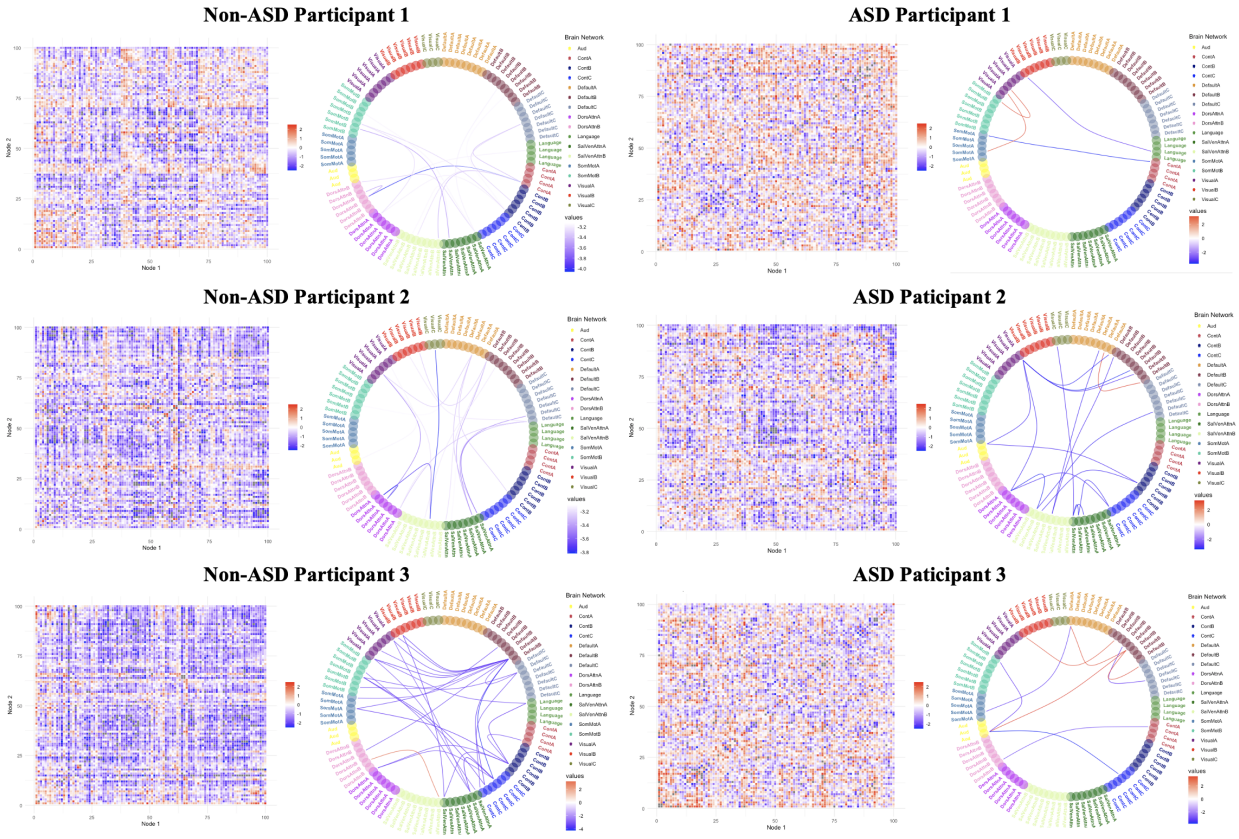

Figure 5: Subject Z-Statistics $\boldsymbol{Z}_{i,\hat{\boldsymbol{B}}_{i2}-\hat{\boldsymbol{B}}_{i1}}$ for Dynamic Brain Functional Connectivity Linear Effects between $\hat{\boldsymbol{B}}_{i2}$ versus $\hat{\boldsymbol{B}}_{i2}$: Heatmap representation of $\boldsymbol{Z}_i$ across 100 by 100 brain region edge. The circle plots show the connectivity edge surpassing the 0.001 significant threshold ($P < 0.001$). The circle border shows 17 brain functional networks.

.

The matrices on the left of each pair show the connectivity patterns within the brain, where each square represents a connection between two regions. The colors in the matrix indicate the strength of the connections. More saturated colors signify stronger connections, while lighter colors indicate weaker connections. The circular graphs on the right, known as connectograms, visualize connections across different brain regions. The red lines represent the positive strength of connectivity, while the blue lines indicate negative connectivity. The segments around the circle correspond to 17 brain functional networks.

The heatmaps demonstrate considerable variation in the associations of eye-tracking events with dynamic functional connectivity among both ASD and non-ASD participants. The patterns of Z-statistics suggest the connectivity associations may be unique for each person. In the non-ASD group, most connectivity coefficients are negative, suggesting that eye fixations have a lesser impact on the dynamics of functional connectivity compared to eye blinks. Conversely, for the ASD group, the connectivity coefficients are a mix of negative and positive values, indicating eye fixations appear to exert a greater influence on the patterns of functional connectivity for some regions.

5.3.2 Population-level associations between dynamic functional connectivity and eye-tracking events

Figure 6 illustrates the group effects $\bar{\boldsymbol{Z}}_{non-ASD}$ for the non-ASD group and $\bar{\boldsymbol{Z}}_{ASD}$ for the ASD group. The figure depicts heatmap plots in the left column and chord diagrams in the right column, where red lines represent $\bar{\boldsymbol{Z}}_{vv'} > 0$ and blue lines indicate $\bar{\boldsymbol{Z}}_{vv'} < 0$. Red lines suggest that the dynamics of functional connectivity are more associated with eye-fixation events than eye-blink events, whereas blue lines suggest that the dynamics of functional connectivity are more influenced by eye-blink events.

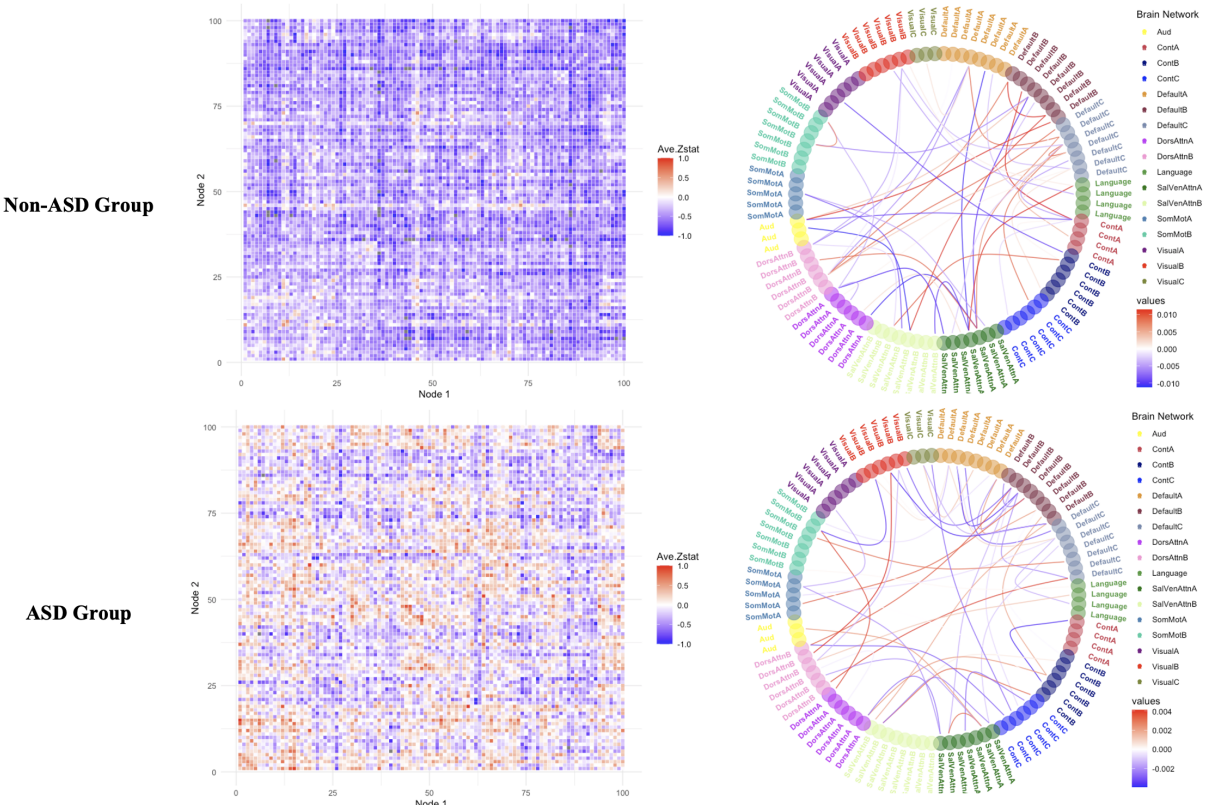

Figure 6: Population level's Z-Statistics $\bar{\boldsymbol{Z}}$ for Dynamic Brain Functional Connectivity Linear Effects between $\hat{\boldsymbol{B}}_{i2}$ and $\hat{\boldsymbol{B}}_{i2}$ in ASD vs. non-ASD group. **Left**: Heatmap representation of $\bar{\boldsymbol{Z}}_i$ across 100 by 100 brain region pairs. **Right**: Circle plots depict the pairs of brain regions selected by absolute $\bar{\boldsymbol{Z}}_{vv'}$ fall into the 1^{st} quartile. **Top**: non-ASD group mean effects $\bar{\boldsymbol{Z}}_{non-ASD}$. **Bottom**: ASD group mean effects $\bar{\boldsymbol{Z}}_{ASD}$. The circle border shows 17 brain functional networks.

The heatmap in Figure 6 illustrates that the brain's dynamic functional connectivity in the non-ASD group is more associated with eye-blink events, as evidenced by predominantly negative $\bar{\boldsymbol{Z}}_{non-ASD}$ coefficients across most regions. Conversely, the ASD group exhibits a more even distribution of $\bar{\boldsymbol{Z}}_{ASD}$ coefficients, spanning both negative and positive values, indicating varied brain connectivity when comparing between eye-blink and eye-fixation events. This observation aligns with the individual-specific dynamic functional connectivity patterns

discussed in the previous section.

Filtering for the first quartile based on the absolute $\bar{\boldsymbol{Z}}_{vv'}$ to visualize on the circle plot in the right column, participants with ASD demonstrate positive connectivity within the somatomotor network and dorsal attention network, in contrast to the non-ASD group. Furthermore, individuals with ASD do not exhibit positive connectivity within the Default Mode Network, diverging from general patterns observed. These insights indicate a broad spectrum of functional connectivity dynamics within ASD. The alterations in these brain networks, consistent with findings from previous research, will be explored further in the discussion section.

6 Discussion

6.1 Non-ASD group: Brain activation associated with eye-tracking events

The analysis in Figure 3 indicates that eye-blink and eye-fixation events are associated with distinct functional activations within brain networks involved in sensory integration, attention deployment, and language processing. Specifically, eye-blink events significantly activate areas like the RH Default Mode Network, associated with introspective and social cognitive processes, and parts of the Visual Area, crucial for the basic processing of visual stimuli. These preliminary results align with previous research indicating that eye-blinking is related to central dopamine function in Jongkees and Colzato (2016), as well as visual stimulus processing in Crnovrsanin et al. (2014). Furthermore, the LH Salience Network, important for distinguishing relevant from irrelevant stimuli and involved in processing reward, motivation, emotion, and pain, is notably activated. Additionally, a Control Network, responsible for high-level executive functions and goal-directed behaviors, is activated during eye-blinks in non-ASD children.

Conversely, eye-fixation events are associated with the brain's visual processing areas across both hemispheres. Notably, both of the LH and RH Language Processing Areas are involved, suggesting the integration of visual information with language and semantic processing (Tanenhaus, 2007; Cooper, 1974). The engagement of both hemispheres' Salience Networks points to the ongoing assessment of visual stimuli's significance, while the Default Mode Networks might relate to internal narratives or daydreaming that can occur during sustained visual fixation (Henderson et al., 2015).

The comparison between eye-fixation and eye-blink events reveals significant differences in the Somatomotor Areas, which are traditionally associated with body movement and sensory information integration. This may highlight the role of motor control and sensory integration in managing and executing eye movements. Furthermore, observed differences in the Salience and Control Networks in response to these events hint at shifts in attention allocation, along with the processing and prioritization of task-relevant stimuli.

6.2 Comparative analysis: Modification in brain activation during eye-tracking in ASD

The findings described in Figure 4 reveal no significant differences in brain functional activities between ASD and non-ASD participants during eye-blink events, using a significance threshold of 0.2. However, the figure highlights notable differences in specific brain regions in response to eye-fixation events. In the Left Hemisphere, Somatomotor Areas A and B, involved in body movement coordination and sensory information processing, show distinct activation. The Default Mode Network B, associated with self-referential thoughts and mind-wandering, the Auditory Cortex, key for sound processing, and the Control Network B, important for executive functions and attention regulation, also respond significantly to eye-fixation events. In the Right Hemisphere, differences are observed in the Salience/Ventral Attention Network A and B, crucial for detecting and filtering relevant stimuli; the Default Mode Network A; the Language Processing Areas, essential for language comprehension and production; and the Somatomotor Area B. These differences indicate a diminished sensitivity in ASD participants to eye-tracking events, particularly eye-fixation events, which is consistent with previous studies (Cheng et al., 2021; Orefice, 2020).

Furthermore, a notable difference is only observed in the RH Language Processing Area when comparing neural activation associated with eye-fixation versus eye-blink between ASD and non-ASD groups, suggesting that ASD participants exhibit a less pronounced distinction between these events in Language Processing activation. This finding is also corresponding to the previous studies (Knaus et al., 2008; Verly et al., 2014; Kleinhans et al., 2008). This may reflect differences in the integration and processing of visual and linguistic information between ASD and non-ASD individuals.

All observed differences suggest that ASD children display lower brain functional activations during eye-tracking events compared to non-ASD children. Reduced sensitivity (functional integration) associated with default and higher-order visual regions in ASD was found in Rudie et al. (2013). Our finding suggests that non-ASD individuals may exhibit greater neural activation associated with eye-fixation events during the movie watching tasks, potentially reflecting an adaptable mechanism of sensory processing and attention. In contrast, the neural activity associated with eye-fixtion versus eye-blink in the ASD group shows a more similar activation pattern during the movie wathcing tasks. In other words, there was less variation in brain activation between different eye-tracking events within sensory and attentional processing regions.

6.3 Initial covariance regression findings

The analysis of individual-level covariance effects reveals that brain functional connectivity is unique to each individual, suggesting the necessity for customized, person-specific interventions. This finding emphasizes the critical role of personalized approaches in comprehensively understanding and effectively addressing brain connectivity issues in ASD. The significance of individual differences in fMRI studies and the call for personalized medicine practices were also noted and advocated for in Dubois and Adolphs (2016).

The observed differences in dynamic functional connectivity alterations during eye-fixation events between ASD and non-ASD groups may suggest underlying differences in information

processing within the brain. Our preliminary findings indicates more pronounced effects of eye-blink effects versus eye-fixation events in the non-ASD group, whereas there was a mix of positive and negative coefficients in the ASD group. Although additional research is necessary, this could imply an alternative utilization of neural resources for processing external stimuli in individuals with ASD.

Notably, in the ASD group, no brain networks exclusively exhibit negative or positive functional connectivity; rather, a balance of negative and positive values is observed across almost all brain networks. In contrast to the non-ASD group, connectivity between regions such as dorsal attention B, Visual B, Somatomotor B, and Default B in ASD group showed positive linear effects when contrasting eye-fixation and eye-blink events, suggesting a bigger difference in connectivity during eye-tracking events in these brain areas. In other words, the connectivity between these brain areas are higher associated with eye-fixation events compared to eye-blink events.

Conversely, in the ASD group, the difference in connectivity between eye-fixation and eye-blink events is notably less pronounced, especially within the Default and language regions. Specifically, connectivity between the Default and language processing areas during eye-fixation events is reduced compared to eye-blink events in individuals with ASD.

The Somatomotor B regions, known for their role in integrating sensory input with motor responses and orchestrating movement planning, together with the Dorsal Attention B and Visual B areas, which are instrumental in directing attention and processing visual stimuli, as well as the Default Mode Network B and language processing areas, play significant roles in cognitive and sensory functions. Our group-level covariance analysis reveals obvious variability in the connectivity of these regions in individuals with ASD, indicating altered neural mechanisms associated with eye-tracking events during movie-watching tasks. These preliminary findings emphasize the crucial need to consider such variability in future research and clinical practices, particularly in the context of ASD, where these brain areas are essential for a range of cognitive, sensory, and motor functions.

7 Conclusion

Our study demonstrates that utilizing eye-blink and eye-fixation events as predictors in fMRI studies of ASD can reveal assocations with brain activation and connectivity. The underlying assumption—that eye-blink events signify less engagement, whereas eye-fixation events indicate engagement—facilitates the identification of unique brain activation regions. Second, the association between brain functional activations and eye-blink events was similar in ASD and non-ASD participants, but differences are significant in their response to eye-fixation events, especially in areas of the brain responsible for sensory processing and attention. These findings indicate a diminished association in ASD to such eye movements, with variations in areas involved in language processing highlighting different ways of integrating visual and linguistic information. Third, we find that the relationship between eye-fixation events and dynamic connectivity appear to vary between individuals. ASD may engage different neural regulatory mechanisms, and sensory and cognitive processes may be managed differently in ASD compared to non-ASD individuals.

It is worth mentioning that these findings are initial steps in understanding the differences

in dynamic functional connectivity between ASD and non-ASD groups. These observations will need more detailed study and confirmation through ongoing research and analysis.

8 Limitations and future directions

Our research, as detailed in this thesis, has several limitations. First, our study is based on a limited number of participants (12 ASD and 22 non-ASD), which may affect the applicability of our findings to a broader population and the reliability of our results.

Second, the use of the Schaefer 100 brain region segmentation we adopted may not be sufficient to detect localized neural activities. Averaging data within each brain region can reduce variance, which is helpful in studies with small sample sizes, but it also compromises the spatial precision of our BOLD signal measurements.

Third, the statistical techniques we employed, particularly in modeling covariance, can be further improved. Notably, the assumption of normality within OLS models does not always hold, especially for data from adjacent brain regions. We use the log-Euclidean transformation and heteroscedasticity consistent standard errors to address normality assumptions, but additional research should investigate this framework. Simulations to validate the accuracy of our approach would be helpful.

Furthermore, our study assumes a simplistic model for the covariance dynamics of functional connectivity, which may not fully capture the complexity of brain interactions. Investigating alternative covariance structures could provide more insightful analyses.

Additionally, future research should investigate eigenvalue decompositions of our estimated coefficient matrices, $\hat{\boldsymbol{B}}_{ij}$. Such decompositions could reveal patterns in the data, offering an understanding of the components influencing brain connectivity. This analysis could improve the interpretability and computational efficiency of models dealing with the high-dimensional data in neuroimaging studies.

9 Acknowledgments

We thank Dr. Sarah Robillard Shultz of the Department of Pediatrics at Emory University School of Medicine, Dr. Kate Revill at the FERN imaging center, Zihang Wang, and the research staff who collected these data, especially Jamie Kortanek and Sydney Olson.

This research was supported in part by the National Institute of Mental Health of the National Institutes of Health under award number R01 MH129855. The content is solely the responsibility of the authors and does not necessarily represent the official views of the National Institutes of Health.

References

Biswal, B. B., Mennes, M., Zuo, X.-N., Gohel, S., Kelly, C., Smith, S. M., Beckmann, C. F., Adelstein, J. S., Buckner, R. L., Colcombe, S., et al. (2010). Toward discovery science of human brain function. *Proceedings of the national academy of sciences*, 107(10):4734–4739.

Braden, B. B., Smith, C. J., Thompson, A., Glaspy, T. K., Wood, E., Vatsa, D., Abbott, A. E., McGee, S. C., and Baxter, L. C. (2017). Executive function and functional and structural brain differences in middle-age adults with autism spectrum disorder. *Autism Research*, 10(12):1945–1959.

Cheng, H.-J., Ng, K. K., Qian, X., Ji, F., Lu, Z. K., Teo, W. P., Hong, X., Nasrallah, F. A., Ang, K. K., Chuang, K.-H., et al. (2021). Task-related brain functional network reconfigurations relate to motor recovery in chronic subcortical stroke. *Scientific Reports*, 11(1):8442.

Cooper, R. M. (1974). The control of eye fixation by the meaning of spoken language: a new methodology for the real-time investigation of speech perception, memory, and language processing. *Cognitive psychology*.

Crnovrsanin, T., Wang, Y., and Ma, K.-L. (2014). Stimulating a blink: reduction of eye fatigue with visual stimulus. In *Proceedings of the SIGCHI conference on human factors in computing systems*, pages 2055–2064.

Di, X. and Biswal, B. B. (2017). Psychophysiological interactions in a visual checkerboard task: reproducibility, reliability, and the effects of deconvolution. *Frontiers in neuroscience*, 11:285356.

Dubois, J. and Adolphs, R. (2016). Building a science of individual differences from fmri. *Trends in cognitive sciences*, 20(6):425–443.

Eack, S. M., Wojtalik, J. A., Keshavan, M. S., and Minshew, N. J. (2017). Social-cognitive brain function and connectivity during visual perspective-taking in autism and schizophrenia. *Schizophrenia research*, 183:102–109.

Elliott, M. L., Knodt, A. R., Cooke, M., Kim, M. J., Melzer, T. R., Keenan, R., Ireland, D., Ramrakha, S., Poulton, R., Caspi, A., et al. (2019). General functional connectivity: Shared features of resting-state and task fmri drive reliable and heritable individual differences in functional brain networks. *Neuroimage*, 189:516–532.

Engle, R. (2002). Dynamic conditional correlation: A simple class of multivariate generalized autoregressive conditional heteroskedasticity models. *Journal of Business & Economic Statistics*, 20(3):339–350.

Esteban, O., Markiewicz, C. J., Blair, R. W., Moodie, C. A., Isik, A. I., Erramuzpe, A., Kent, J. D., Goncalves, M., DuPre, E., Snyder, M., et al. (2019). fmriprep: a robust preprocessing pipeline for functional mri. *Nature methods*, 16(1):111–116.

Friston, K. J., Frith, C. D., Liddle, P. F., and Frackowiak, R. S. (1993). Functional connectivity: the principal-component analysis of large (pet) data sets. *Journal of Cerebral Blood Flow & Metabolism*, 13(1):5–14.

Friston, K. J., Harrison, L., and Penny, W. (2003). Dynamic causal modelling. *Neuroimage*, 19(4):1273–1302.

Friston, K. J., Holmes, A. P., Worsley, K. J., Poline, J.-P., Frith, C. D., and Frackowiak, R. S. (1994). Statistical parametric maps in functional imaging: a general linear approach. *Human brain mapping*, 2(4):189–210.

Greene, A. S., Gao, S., Scheinost, D., and Constable, R. T. (2018). Task-induced brain state manipulation improves prediction of individual traits. *Nature communications*, 9(1):2807.

Henderson, J. M., Choi, W., Luke, S. G., and Desai, R. H. (2015). Neural correlates of fixation duration in natural reading: Evidence from fixation-related fmri. *NeuroImage*, 119:390–397.

Hoff, P. D. and Niu, X. (2012). A covariance regression model. *Statistica Sinica*, pages 729–753.

Huijbers, W., Van Dijk, K. R., Boenniger, M. M., Stirnberg, R., and Breteler, M. M. (2017). Less head motion during mri under task than resting-state conditions. *Neuroimage*, 147:111–120.

Hull, J. V., Dokovna, L. B., Jacokes, Z. J., Torgerson, C. M., Irimia, A., and Van Horn, J. D. (2017). Resting-state functional connectivity in autism spectrum disorders: a review. *Frontiers in psychiatry*, 7:205.

Jongkees, B. J. and Colzato, L. S. (2016). Spontaneous eye blink rate as predictor of dopamine-related cognitive function—a review. *Neuroscience & Biobehavioral Reviews*, 71:58–82.

Kleinhans, N. M., Müller, R.-A., Cohen, D. N., and Courchesne, E. (2008). Atypical functional lateralization of language in autism spectrum disorders. *Brain research*, 1221:115–125.

Knaus, T. A., Silver, A. M., Lindgren, K. A., Hadjikhani, N., and Tager-Flusberg, H. (2008). fmri activation during a language task in adolescents with asd. *Journal of the International Neuropsychological Society*, 14(6):967–979.

Lindquist, M. A., Xu, Y., Nebel, M. B., and Caffo, B. S. (2014). Evaluating dynamic bivariate correlations in resting-state fmri: a comparison study and a new approach. *NeuroImage*, 101:531–546.

Lombardo, M. V., Eyler, L., Moore, A., Datko, M., Barnes, C. C., Cha, D., Courchesne, E., and Pierce, K. (2019). Default mode-visual network hypoconnectivity in an autism subtype with pronounced social visual engagement difficulties. *eLife*, 8:e47427.

Long, J. S. and Ervin, L. H. (2000). Using heteroscedasticity consistent standard errors in the linear regression model. *The American Statistician*, 54(3):217–224.

Maenner, M. J. (2023). Prevalence and characteristics of autism spectrum disorder among children aged 8 years—autism and developmental disabilities monitoring network, 11 sites, united states, 2020. *MMWR. Surveillance Summaries*, 72.

Marsman, J. B. C., Renken, R., Velichkovsky, B. M., Hooymans, J. M., and Cornelissen, F. W. (2012). Fixation based event-related fmri analysis: Using eye fixations as events in functional magnetic resonance imaging to reveal cortical processing during the free exploration of visual images. *Human Brain Mapping*, 33(2):307–318.

McLaren, D. G., Ries, M. L., Xu, G., and Johnson, S. C. (2012). A generalized form of context-dependent psychophysiological interactions (gppi): a comparison to standard approaches. *Neuroimage*, 61(4):1277–1286.

Meissner, T. W., Walbrin, J., Nordt, M., Koldewyn, K., and Weigelt, S. (2020). Head motion during fmri tasks is reduced in children and adults if participants take breaks. *Developmental cognitive neuroscience*, 44:100803.

Mejia, A. F., Yue, Y. R., Bolin, D., Lindgren, F., and Lindquist, M. A. (2019). A bayesian general linear modeling approach to cortical surface fmri data analysis. *Journal of the American Statistical Association*.

Orefice, L. L. (2020). Peripheral somatosensory neuron dysfunction: emerging roles in autism spectrum disorders. *Neuroscience*, 445:120–129.

Park, K. Y., Lee, J. J., Dierker, D., Marple, L. M., Hacker, C. D., Roland, J. L., Marcus, D. S., Milchenko, M., Miller-Thomas, M. M., Benzinger, T. L., et al. (2020). Mapping language function with task-based vs. resting-state functional mri. *PLoS One*, 15(7):e0236423.

Pham, D. D., Muschelli, J., and Mejia, A. F. (2022). ciftitools: A package for reading, writing, visualizing, and manipulating cifti files in r. *NeuroImage*, 250:118877.

R Core Team (2024). *R: A Language and Environment for Statistical Computing*. R Foundation for Statistical Computing, Vienna, Austria.

Rahko, J. S., Vuontela, V. A., Carlson, S., Nikkinen, J., Hurtig, T. M., Kuusikko-Gauffin, S., Mattila, M.-L., Jussila, K. K., Remes, J. J., Jansson-Verkasalo, E. M., et al. (2016). Attention and working memory in adolescents with autism spectrum disorder: a functional mri study. *Child Psychiatry & Human Development*, 47:503–517.

Rajagopal, A., Byars, A., Schapiro, M., Lee, G., and Holland, S. (2014). Success rates for functional mr imaging in children. *American Journal of Neuroradiology*, 35(12):2319–2325.

Ranti, C., Jones, W., Klin, A., and Shultz, S. (2020). Blink rate patterns provide a reliable measure of individual engagement with scene content. *Scientific reports*, 10(1):8267.

Ripley, B. D. (2002). Time series in r 1.5. 0. *The Newsletter of the R Project Volume*, 2:2.

Risk, B. B., Murden, R. J., Wu, J., Nebel, M. B., Venkataraman, A., Zhang, Z., and Qiu, D. (2021). Which multiband factor should you choose for your resting-state fmri study? *NeuroImage*, 234:117965.

Rudie, J. D., Brown, J., Beck-Pancer, D., Hernandez, L., Dennis, E., Thompson, P., Bookheimer, S., and Dapretto, M. (2013). Altered functional and structural brain network organization in autism. *NeuroImage: clinical*, 2:79–94.

Satterthwaite, T. D., Elliott, M. A., Gerraty, R. T., Ruparel, K., Loughead, J., Calkins, M. E., Eickhoff, S. B., Hakonarson, H., Gur, R. C., Gur, R. E., et al. (2013). An improved framework for confound regression and filtering for control of motion artifact in the preprocessing of resting-state functional connectivity data. *Neuroimage*, 64:240–256.

Schaefer, A., Kong, R., Gordon, E. M., Laumann, T. O., Zuo, X.-N., Holmes, A. J., Eickhoff, S. B., and Yeo, B. T. (2018). Local-global parcellation of the human cerebral cortex from intrinsic functional connectivity mri. *Cerebral cortex*, 28(9):3095–3114.

Schwartzman, A. (2016). Lognormal distributions and geometric averages of symmetric positive definite matrices. *International statistical review*, 84(3):456–486.

Tanenhaus, M. K. (2007). Eye movements and spoken language processing. In *Eye Movements*, pages 443–II. Elsevier.

Vanderwal, T., Eilbott, J., and Castellanos, F. X. (2019). Movies in the magnet: Naturalistic paradigms in developmental functional neuroimaging. *Developmental cognitive neuroscience*, 36:100600.

Verly, M., Verhoeven, J., Zink, I., Mantini, D., Peeters, R., Deprez, S., Emsell, L., Boets, B., Noens, I., Steyaert, J., et al. (2014). Altered functional connectivity of the language network in asd: role of classical language areas and cerebellum. *NeuroImage: Clinical*, 4:374–382.

Welvaert, M., Durnez, J., Moerkerke, B., Verdoolaege, G., and Rosseel, Y. (2011). neurosim: An r package for generating fmri data. *Journal of Statistical Software*, 44(10):1–18.

Worsley, K. J., Liao, C. H., Aston, J., Petre, V., Duncan, G., Morales, F., and Evans, A. C. (2002). A general statistical analysis for fmri data. *Neuroimage*, 15(1):1–15.

Zhao, W., Makowski, C., Hagler, D. J., Garavan, H. P., Thompson, W. K., Greene, D. J., Jernigan, T. L., and Dale, A. M. (2023). Task fmri paradigms may capture more behaviorally relevant information than resting-state functional connectivity. *NeuroImage*, 270:119946.

Zumer, J. M., Brookes, M. J., Stevenson, C. M., Francis, S. T., and Morris, P. G. (2010). Relating bold fmri and neural oscillations through convolution and optimal linear weighting. *Neuroimage*, 49(2):1479–1489.